International Journal of Thermal Sciences 88 (2015) 1-6

On the use of classical JMAK crystallization kinetic theory to describe simultaneous processes leading to the formation of different phases in metals

J. S. Blázquez, C. F. Conde, A. Conde

Dpto. Física de la Materia Condensada, Universidad de Sevilla, ICMSE-CSIC. P.O. Box 1065, 41080, Sevilla, Spain

Abstract

The classical theory of Johnson-Mehl-Avrami-Kolmogorov (JMAK) is widely used to describe the kinetics of crystallization even when the premises required for its application are not strictly fulfilled. In this paper we propose a procedure to obtain the JMAK parameters of the independent transformations that simultaneously occur during a crystallization process (e.g. leading to the formation of several crystalline phases). The predictions of the analysis have been used to describe the crystallization process of two amorphous alloys with $Fe_{90}Zr_{10}$ and $(Fe_{0.7}Co_{0.3})Zr_{10}$ composition, respectively, which consists of two overlapped processes ascribed to the formation of α-Fe(Co) phase and a Zr-rich intermetallic.

Keywords: Johnson-Mehl-Avrami-Kolmogorov theory, Avrami exponent, crystallization kinetics, glassy material.

Corresponding author: J. S. Blázquez

Tel: +34 954 55 60 29

1 Introduction

Phase transformation kinetics affects numerous working fields in Materials Science as solid state transformations usually imply changes in the properties and characteristics of the systems. In some cases, these changes can be advantageous (e.g. in order to use the material as a sensor), however, in other cases, phase transformations must be avoided to keep the specific microstructure responsible for the desired properties. This is particularly important in the case of metastable systems (such as crystallization of amorphous alloys [1,2,3,4,5], polymers [6,7,8] and other glasses [9,10]), for which the metastable state should not be easily recovered once the transformation occurs. Therefore, understanding the mechanisms affecting the transformation kinetics is a key point in order to optimize the systems or to establish a comparison on the performance and perspectives of lifetime of a certain device. In this sense, it is particularly interesting the use of simple kinetic models based on average behaviors, which describe the main features of the transformation using only a few parameters. This can explain the success of using the classical theory based on nucleation and growth.

The development of the classical crystallization model (JMAK theory) can be ascribed to the works of Johnson and Mehl [11], Avrami [12] and Kolmogorov [13] at the middle of the XXth century. This theory, developed for isothermal processes, describes the variation of the transformed fraction with the annealing time based on simple laws of nucleation and growth. In order to be described by JMAK theory, a transformation should fulfill the five postulates of Kolmogorov [14]:

1 Initially, a parent phase exists, which is progressively substituted by the product phase;

2 the volume of any formed grain is much smaller than the whole volume of the system;

3 the nucleation is random;

4 the shape of the new crystals is convex; and

5 the linear growth can be expressed as a product of a time dependent function and a direction dependent function.

The two latter postulates can be assumed if isotropic growth of spherical crystals is considered. In this sense, potential laws can be used to describe the nucleation and growth rates as: $I(t)=I_0 t^b$ and $G(t)=G_0 t^a$, respectively, where I_0, G_0, b and a are constants and t is the time. Neglecting the geometrical impingement [15], the extended transformed fraction, X^*, in three dimension growth processes can be obtained as the integration from time 0 to t of the relative volume growth by each grain formed at time t':

$$X^* = \frac{4\pi}{3}\int_0^t I(t')\left(\int_{t'}^t G(\tau)\,d\tau\right)^3 dt' = \frac{4\pi}{3}\frac{I_0 G_0^{\,3}}{C} t^{3(a+1)+b+1} \tag{1}$$

where C is a function of the parameters a and b. The prefactors can be considered together and a simpler relation is finally obtained:

$$X^* = (kt)^n \tag{2}$$

where k is the frequency factor and the parameter n is the Avrami exponent, which contains information about the type of nucleation and growth processes implied in the transformation: $n=n_I+3\cdot n_G$, where n_I corresponds to nucleation and n_G to growth. Decreasing and increasing nucleation rates have been considered in the previous analysis ($b<0$ and $b>0$, respectively), although the way it changes is fixed along the transformation by the power law. Moreover, the theory of crystallization describes diffusion controlled growth processes with $n_G=1/2$ and interface controlled growth processes with $n_G=1$ [16].

As the transformation proceeds, the different transformed regions might overlap and this will lead to an overestimation of the transformed fraction described by X^*. However, the extended transformed fraction is still very helpful by using statistical criteria to correlate it with the actual transformed fraction, X:

$$\frac{dX}{dX^*} = 1 - X \tag{3}$$

Considering that $X^*=0$ implies $X=0$, from integrating Eq. (3) we obtain:

$$X = 1 - \exp\left(-X^*\right) \tag{4}$$

And the well-known JMAK equation is obtained substituting Eq. (2) in Eq. (4)

$$X = 1 - \exp\left(-\left(kt\right)^n\right) \tag{5}$$

A stronger impingement than that purely geometrical reflected by Eq.(3) can be considered using a general equation instead of Eq. (3) [17]:

$$\frac{dX}{dX*} = \left(1 - X\right)^{1+c} \tag{6}$$

Where the impingement parameter $c=1$ will lead to the Austin-Rickett equation [16]. A general solution for $c\neq 0$ can be found in Ref. [18].

All this theory is developed to describe simple crystallization processes, where a single phase is formed. However, JMAK theory as well as the Avrami exponent are extensively used to describe and compare different types of experimental transformations. In this paper, we explore how the application of JMAK analysis to multiple processes necessarily implies deviations in the experimental Avrami exponents with respect to the actual values and we propose a method to extract these actual values. The present analytical method can be of interest particularly for researchers working in the field of solidification and crystallization modelling.

2 Aplication of JMAK analysis to multiple transformation processes

Although the requirements for using JMAK theory are strict, its extension beyond these limits is generally used. In this sense it is worth noticing that the transformations can imply the

formation of different product phases and, therefore, two possibilities arise for calculation of the total transformed fraction [19]:

a) The transformations can be independent between them, i.e. the product phases do not compete for the same type of atoms and the actual transformed fraction is just the addition of the contributions of each phase:

$$X = \sum f_i X_i = \sum f_i \left(1 - \exp\left\{-\left(k_i \left(t - t_{0i}\right)\right)^{n_i}\right\}\right) \tag{7}$$

where $\sum f_i = 1$, being f_i the maximum transformed fraction of the total volume of the sample corresponding to the i process and k_i, t_{0i} and n_i being the frequency factor, the induction time and the Avrami exponent of the i process, respectively.

b) The transformations can be dependent and the progress of one of the product phases depends on the degree of transformation of the others. In this case the extended transformed fraction is obtained by addition of the individual ones:

$$X^* = \sum X_i^* \tag{8}$$

and thus the actual transformed fraction is obtained applying equation (5) to this total extended transformed fraction:

$$X = 1 - \exp\left\{-\sum \left(k_i \left(t - t_{0i}\right)\right)^{n_i}\right\} \tag{9}$$

This expression implies that the final phase fraction depends on the annealing conditions (for isothermal treatments) or the heating rate (for non-isothermal treatments) and cannot lead to decoupled processes [19], because the available untransformed volume for each product phase is shared with the others. Therefore, the first transformation to occur will progressively decrease the available volume and if the other processes are sufficiently delayed (e.g. due to a high activation energy and a high heating rate) they might not occur at all. This

possibility was explored in a previous paper [19], finding some relationships between the activation energies and the heating rate dependence of the local Avrami exponent.

In this work we will describe the dependence of the effective local Avrami exponent, n^*, with the transformed fraction, X, in multiple processes leading to the formation of non-competitive product phases, which can be described using Eq. (7) and where:

$$n^* = \frac{d\ln\left(-\ln\left(1-X\right)\right)}{d\ln\left(t-t_0^*\right)} = \sum_i \frac{d\ln\left(-\ln\left(1-X\right)\right)}{d\ln\left(-\ln\left(1-X_i\right)\right)} \frac{d\ln\left(-\ln\left(1-X_i\right)\right)}{d\ln\left(t-t_0^*\right)} \tag{10}$$

where t_0^* is the effective induction time (which should correspond to the induction time of the earlier process). In a first approximation, for two non-overlapped processes, the transformed fraction can be described as:

$$X = \begin{cases} fX_1 & \text{if } X < f \\ f + \left(1-f\right)X_2 & \text{if } X > f \end{cases} \tag{11}$$

where f is the maximum transformed fraction achieved by the first process. Under this approximation, the value of the effective local Avrami exponent of the complete transformation, n^*, can be obtained in two independent X ranges by differentiating ln(-ln(1-X)) with respect to ln(t) (consider that the corresponding induction times are very small with respect to the annealing time) for $X<f$ and $X>f$. Figure 1a shows, for f=0.6, the local values of the effective Avrami exponent for two processes with different values of n_1 and n_2. The $n^*(X)$ curves are proportional to the corresponding Avrami exponent while their shape is independent. Changes in f should lead to a shift of the kink point to $n^*(f)$=0.

The previous analysis can be easily generalized to N>2 non-overlapped processes:

$$X = \begin{cases} f_1 X_1 & \text{if } X < f_1 \\ \dots & \\ \sum_{i=1}^{m-1} f_i + f_m X_m & \text{if } \sum_{i=1}^{m-1} f_i < X < \sum_{i=1}^{m} f_i \\ \dots & \\ \sum_{i=1}^{N-1} f_i + \left(1 - \sum_{i=1}^{N-1} f_i\right) X_N & \text{if } X > \sum_{i=1}^{N-1} f_i \end{cases} \quad (12)$$

The value of $n^*(X)$ can be obtained by differentiating ln(-ln(1-X)) with respect to ln(t) in the different X ranges as:

$$n^* = n_m \left(\frac{\sum_{i=1}^{m} f_i - X}{1 - X} \right) \frac{\ln\left(\frac{\sum_{i=1}^{m} f_i - X}{f_m} \right)}{\ln(1 - X)} \quad \text{if } \sum_{i=1}^{m-1} f_i < X < \sum_{i=1}^{m} f_i \quad (13)$$

Figure 1b shows the effective local Avrami exponent obtained for three non-overlapped processes for different values of individual n_i. Several features should be mentioned:

1) Only for the earlier process n_1 can be directly identified as the value towards which n^* tends at X=0. However, for the processes occurring in successive steps, the corresponding n_i values are not evident.
2) For an intermediate process, the effective value of the local Avrami exponent, $n^*(X)$, increases with the increase of the corresponding n_i value. However, $n^*(X)$ remains always below n_i. The value of the actual Avrami exponent of the m process, n_m, is related to the local maximum of the effective Avrami exponent, $n^{*\max}$, and the total transformed fraction at this maximum, X^m:

$$n_m = n^{*\max} \left(1 - \frac{1 - \sum_{i=1}^{m} f_i}{\sum_{i=1}^{m} f_i - X^m} \ln\left(1 - X^m\right) \right) \quad (14)$$

3) Finally, in the case of the last process, we can observe that the slope dn*/dX of the n*(X) curve increases as the corresponding n_N increases and its value can be obtained as:

$$n_N = n* - \frac{dn*}{dX}(1-X)\ln(1-X) \tag{15}$$

On the other hand, when Eq. (13) is derived with respect to X in this range, we obtain:

$$\ln(f_N) = -\frac{1}{n_N}(1-X)\left[\ln(1-X)\right]^2 \frac{dn*}{dX} \tag{16}$$

Therefore, combining Eq. (15) and (16), it is possible to obtain both the Avrami exponent of the last process and its corresponding fraction f_N.

3 Comparison to experimental data

In order to test the viability of the proposed analysis, crystallization of two amorphous $Fe_{90}Zr_{10}$ and $(Fe_{0.7}Co_{0.3})_{90}Zr_{10}$ ribbons was studied by differential scanning calorimetry (DSC) using a Perkin-Elmer DSC7 calorimeter at different heating rates. Samples were submitted to continuous heating at 10, 20, 40 and 80 K/min from room temperature up to 993 K. Two standards (melting points of lead and K_2CrO_4) were used to calibrate the calorimeter in a broad temperature range from room temperature to 1000 K at 40 K/min. The effect of the thermal inertia was corrected by measuring the standard samples also at those heating rates different to the one used for calibration. Amorphous ribbons were prepared by melt-spinning technique using an Edmund Bühler SC in argon atmosphere. Both alloys show two slightly overlapped transformations (figure 2) which correspond to the formation of bcc Fe-type nanocrystals and a Zr-rich intermetallic as shown by X-ray diffraction and transmission electron microscopy. Microstructure and magnetic properties of these alloys can be found elsewhere [20].

In order to obtain the *n*(X)* values (figure 3), a direct approach to non-isothermal processes of the JMAK theory is applied [21,19]. This approach allows us to obtain the local

values of the Avrami exponent from a single non isothermal DSC scan but it requires an estimation of the activation energy (which was obtained using Kissinger method [20]). This approach is based on the following approximation:

$$\int_{t_0}^{t} k(T)\,dt = k'(T)\frac{\left(T - T_0'\right)}{\beta} \tag{17}$$

where β is the heating rate. It is worth mentioning that the best approximation is obtained for $T_0' \sim T_p/2$ [19] instead of the onset temperature [21], being T_p the peak temperature. If the correct value of T_0' is not used, the major deviations can be found at very low transformed fractions. It is also important to point out that using $T_0'=0$ K yields only small deviations at very low transformed fractions [19]. It is worth noting that for very small and very high X values the effects of errors in the baseline are more important and, moreover, deviations from the relationship of proportionality between X and the enthalpy registered by DSC can occur at high X values [22]. Therefore, we have excluded these values from our study.

Concerning the earlier process, the trend for the data above X=0.1 as X is reduced indicates values of $n_1 \sim 1.75$ and 2.5 for the Co-free and the Co-containing compositions, respectively. In the case of the Co-containing alloy, this value should indicate a constant nucleation and three dimensional growth controlled by diffusion for the earlier process (formation of α-Fe phase), whereas in the case of the Co-free alloy, the presence of quenched in nuclei could explain a lower value of n_1.

More information can be obtained after applying Eq. (19) and (20) to the second transformation process. Results from these equations (n_2 and f_2, respectively) would be meaningful only in the range where there is no overlapping between the two transformations. Figures 4a and 5a show dX/dT vs. X plots corresponding to the Co-free and the Co-containing alloys where the vertical lines mark the corresponding X ranges for which nearly constant values of n_2 and f_2 are obtained (ranges shown in the lower panels b and c of figures 4 and 5, respectively). As X increases approaching $X \sim 0.9$, the calculated values diverge and thus, as

commented above, we have not considered very high values of X in the analysis. Therefore, n_2=1.74±0.16 and 1.82±0.06 and f_2=0.40±0.04 and 0.35±0.01 for the Co-free (from X=0.75 to 0.85) and the Co-containing (from X=0.8 to 0.85) alloy, respectively (the corresponding range analyzed for X_2 is between ~0.4 and ~0.6).

Finally, once the final fraction of each process is known after determining f_2, it is possible to directly obtain the local values of the individual processes in the regions not affected by the overlapping. This can be done analogously as for n^* but substituting in Eq. (10) X for $X_1=X/(1-f_2)$ or $X_2=[X-(1-f_2)]/f_2$ to obtain n_1 or n_2, respectively. Results are shown in figure 6 for each alloy, where dash-dotted lines show the effective local Avrami exponent, n^*, for comparison. When overlapping between the processes is strong, the proposed analysis cannot be applied, thus there exists an X range for which no values are obtained. Nevertheless, values of the local Avrami exponent are obtained up to X_1~0.9 for the first process and from X_2~0.3 for the second process. The average values of the Avrami exponents (neglecting values below X<0.1 and above X>0.9) are $\langle n_1 \rangle$=1.66±0.14 and 2.36±0.21 and $\langle n_2 \rangle$=1.68±0.06 and 1.73±0.02, for the Co-free and the Co-containing alloys, respectively. These values are in good agreement with the previously estimated ones. Because of TEM images do not show an anisotropic growth of the crystallites [20], the Avrami exponents of the first process could be explained due to three dimensional growth controlled by diffusion for both alloys but with the presence of quenched in nuclei for the Co-free alloy. The low values of the Avrami exponent of the second process in both alloys, ~1.7, could be understood as due to the presence of quenched in nuclei of the intermetallic phase or to a sudden saturation of the nucleation sites for this phase. Moreover, as the total transformed fraction is high along this process, other impingement phenomena than the purely geometrical could be also responsible for such values (i.e. soft impingement [15]). Further detailed studies as annealing time dependency of the microstructure could help to elucidate the processes occurring in this particular case. However, this study is beyond the scope of the present paper, where we wanted to show how to recover the actual values of the Avrami exponent when JMAK theory is directly applied to a non-single process.

5. Conclusions

JMAK theory is widely used and applied to describe transformations which do not strictly fulfill the required premises. However, in this work we have demonstrated that a careful analysis of the local Avrami exponents obtained for transformations implying multiple processes can lead to obtaining the actual parameters of the individual processes.

The predictions of the analysis have been used to describe the crystallization process of two $Fe_{90}Zr_{10}$ and $(Fe_{0.7}Co_{0.3})Zr_{10}$ amorphous alloys, which occurs in two overlapped processes ascribed to the formation of α-Fe(Co) phase and a Zr-rich intermetallic.

Three dimensional diffusion controlled growth is derived for all the transformations involved. Constant nucleation is only inferred for the formation of α-Fe(Co) phase in the Co-containing alloy, whereas a lower Avrami exponent for the Co-free alloy could be due to the presence of quenched in nuclei. The low Avrami exponents ascribed to the second transformation ~1.7, should indicate the same crystallization mechanism for both alloys, which could imply the presence of quenched in nuclei (or a sudden nucleation site saturation) for the intermetallic phase or a stronger impingement than the purely geometrical.

Acknowledgements

This work was supported by the Spanish Ministry of Science and Innovation and EU FEDER (Project MAT2013-45165-P) and the PAI of the Regional Government of Andalucía (Project P10-FQM-6462).

Figure captions

Figure 1. Values of the theoretical effective local Avrami exponent derived for (a) two non-overlapped processes (with f_1=0.6 and f_2=0.4) and (b) three non-overlapped processes (with f_1=0.4, f_2=0.3 and f_3=0.3) as a function of the transformed fraction. The corresponding actual Avrami exponents of the first and second processes, n_1 and n_2, respectively, are indicated.

Figure 2. DSC scans at 40 K/min of the two studied amorphous alloys.

Figure 3. Values of the effective Avrami exponents, n^*, of the two-process transformation observed for the two studied alloys.

Figure 4. (a) Rate of change of the transformed fraction with temperature as a function of the transformed fraction for the $Fe_{90}Zr_{10}$ alloy. Vertical lines mark the range shown in the lower panels. (b) Avrami exponent of the final process calculated from Eq. (19). (c) Maximum transformed fraction corresponding to the second process calculated from Eq. (20).

Figure 5. (a) Rate of change of the transformed fraction with temperature as a function of the transformed fraction for the $(Fe_{0.7}Co_{0.3})_{90}Zr_{10}$ alloy. Vertical lines mark the range shown in the lower panels. (b) Avrami exponent of the final process calculated from Eq. (19). (c) Maximum transformed fraction corresponding to the second process calculated from Eq. (20).

Figure 6. Calculated Avrami exponents for the first and second processes (solid lines) as a function of the total transformed fraction for $Fe_{90}Zr_{10}$ and $(Fe_{0.7}Co_{0.3})_{90}Zr_{10}$ alloys. Values of the effective Avrami exponent for the double process (dotted lines) are shown for comparison.

Figure 1

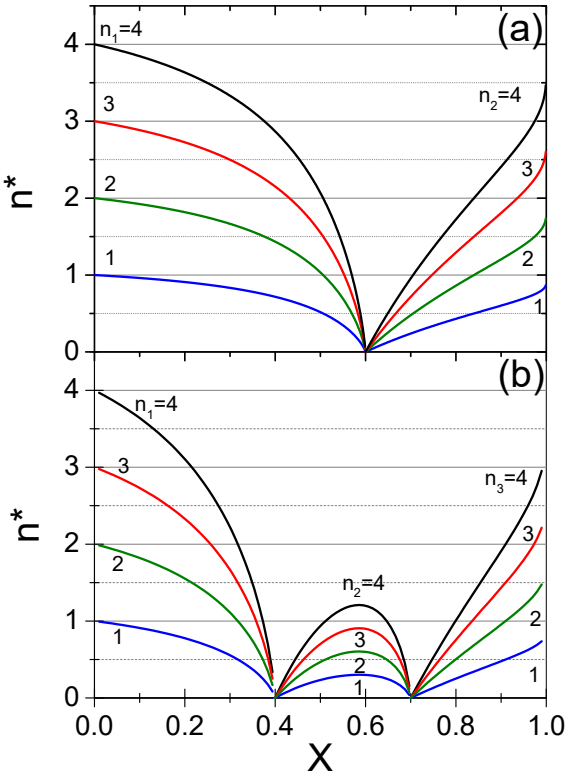

Figure 2

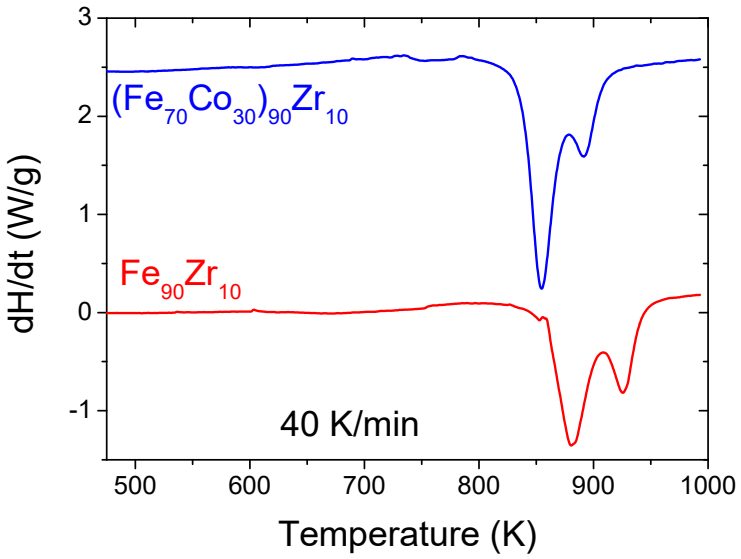
3
2
1
0
-1
dH/dt (W/g)
(Fe70Co30)90Zr10
Fe90Zr10
40 K/min
500
600
700
800
900
1000
Temperature (K)

Figure 3

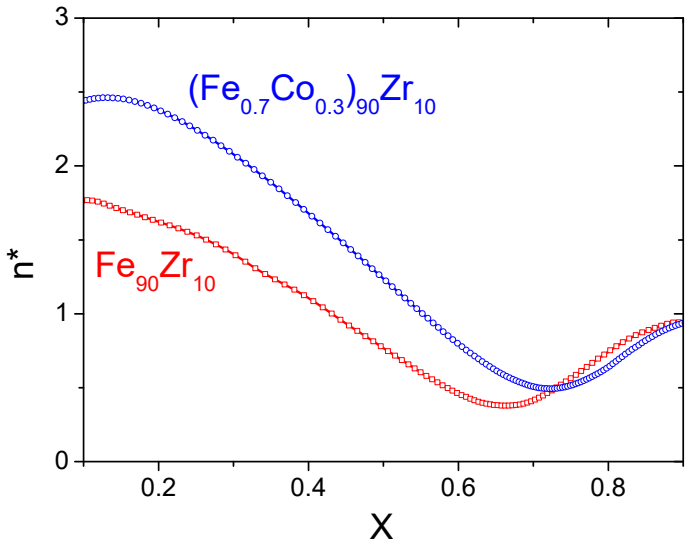

Figure 4

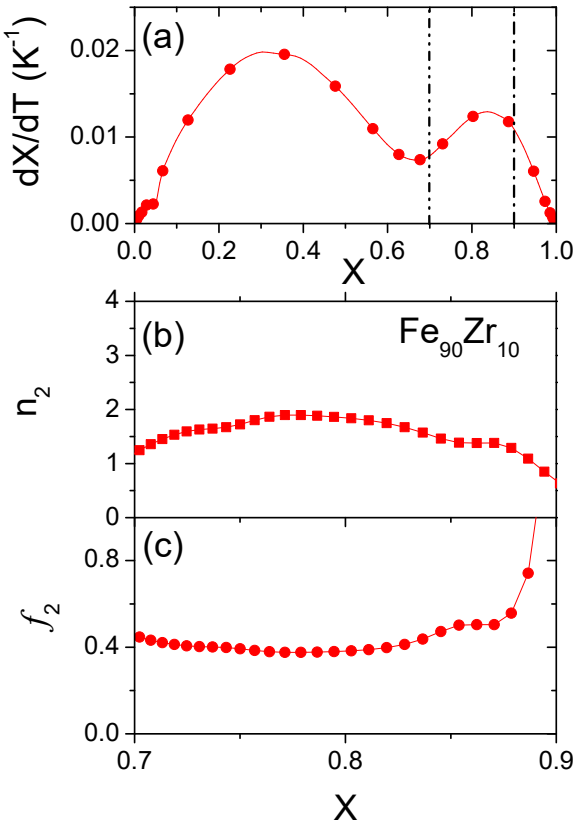
(a)
dX/dT (K^{-1})
0.02
0.01
0.00
0.0
0.2
0.4
0.6
0.8
1.0
X
(b)
Fe$_{90}$Zr$_{10}$
n$_2$
4
3
2
1
0
(c)
f_2
0.8
0.4
0.0
0.7
0.8
0.9
X

Figure 5

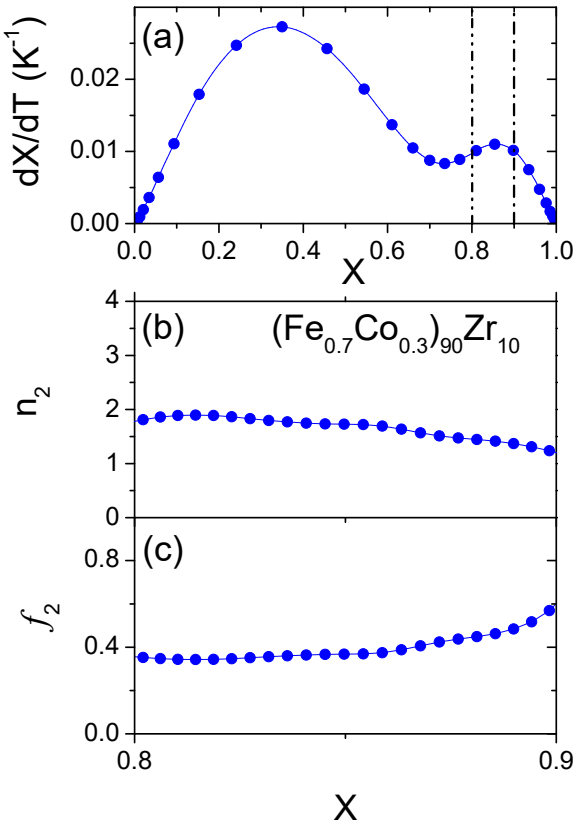
(a)
dX/dT (K^{-1})
0.02
0.01
0.00
0.0
0.2
0.4
0.6
0.8
1.0
X
(b)
(Fe$_{0.7}$Co$_{0.3}$)$_{90}$Zr$_{10}$
n$_2$
4
3
2
1
0
(c)
f_2
0.8
0.4
0.0
0.8
0.9
X

Figure 6

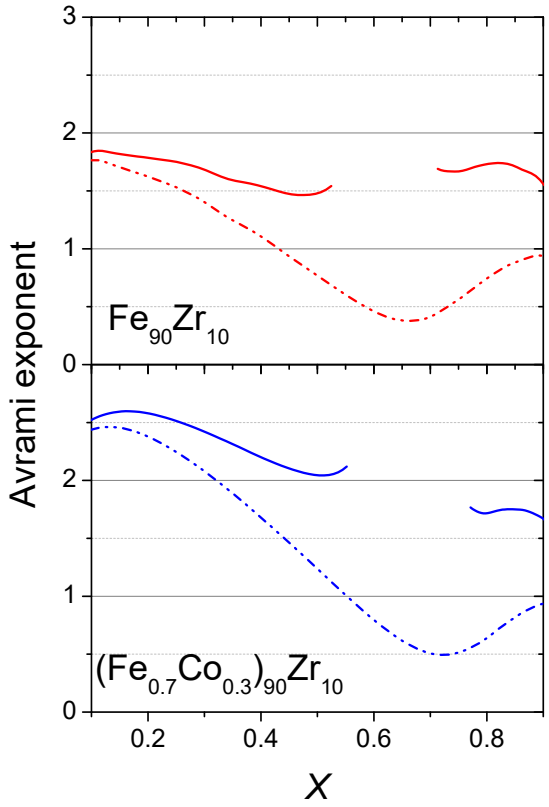

References

[1] C. Yang, L. H. Liu, Y. G. Yao, Y. H. Li, Y. Y. Li, J. All. Comp. 586 (2014) 542-548.
[2] J. Torrens-Serra, I. Peral, J. Rodríguez-Viejo, M. T. Clavaguera-Mora, J. Non-Cryst. Sol. 358 (2012) 107-113.
[3] M. Vasic, D. M. Minic, V. A. Blagojevic, D. M. Minic, Therm. Acta 572 (2013) 45-50.
[4] J. S. Blázquez, C. F. Conde, A. Conde, Appl. Phys. A 76 (2003) 571-575.
[5] J. S. Blázquez, M.Millán, C. F. Conde, A. Conde, 87 (2007) 4151-4167.
[6] P. Zou, S. Tang, Z. Fu, H. Xiong, Int. J. Therm. Sci. 48 (2009) 837-846.
[7] M. L. Di Lorenzo, C. Silvestre, Prog. Mater. Sci. 24 (1999) 917-950.
[8] F. J. Blanco-Rodríguez, J. I. Ramos, Int. J. Therm. Sci. 58 (2012) 102-112.
[9] A. Boutarfaia, M. Legouera, M. Poulain, Int. J. Therm. Sci. 41 (2002)157-162.
[10] M. Fontana, B. Arconde, M. T. Clavaguera-Mora, N. Clavaguera, J. Non-Cryst. Sol. 353 (2007) 2131-2142.
[11] W.A. Johnson, R. F. Mehl, Trans. Am. Inst. Mining Met. Engrs. 135 (1939) 416
[12] M. Avrami, J. Chem. Phys. 9 (1941) 177
[13] A. N. Kolmogorov, Bull. Acad. Sci. USSR, Phys. Ser. 1 (1937) 355
[14] A. A. Burbelko, E. Fras, W. Kapturkiewicz, Mat. Sci. Eng. A 413 (2005) 429-434.
[15] M.T. Clavaguera-Mora, N. Clavaguera, D. Crespo, T. Pradell, Prog. Mater. Sci. 47 (2002) 559-619
[16] J. Burke, The Kinetics of Phase Transformation in Metals (Pergamon Press, Oxford, 1965).
[17] E. S. Lee, Y. G. Kim, Acta Metal. Mater. 38 (1990) 1669–1676.
[18] M. J. Starink, J. Mater. Sci. 36 (2001) 4433–4441.
[19] J. S. Blázquez, J. M. Borrego, C. F. Conde, A. Conde, S. Lozano-Pérez, J. All. Comp. 544 (2012) 73-81.
[20] J. S. Blázquez, J. J. Ipus, C. F. Conde, D. Cabrera, V. Franco, A. Conde, J. All. Comp. (2014), Doi: 10.1016/j.jallcom.2014.01.095
[21] J. S. Blázquez, C. F. Conde, A. Conde, Acta Mater. 53 (2005) 2305-2311.
[22] J. M. Barandiarán, I. Tellería, J. S. Garitaonandía, H. A. Davies, J. Non-Cryst. Sol. 329 (2003) 57-62.